Molecular Catalysis 516 (2021) 111960

Contents lists available at ScienceDirect

Molecular Catalysis

journal homepage: www.journals.elsevier.com/molecular-catalysis

Enhanced oxygen evolution reaction on polyethyleneimine functionalized graphene oxide in alkaline medium

Zafar Khan Ghouri [a,b,c,*], Khaled Elsaid [a], Ahmed Badreldin [a], Mohamed Mahmoud Nasef [c,d], Nurfatehah Wahyuny Che Jusoh [c], Ahmed Abdel-Wahab [a,*]

[a] Chemical Engineering Program, Texas A&M University at Qatar, P.O. 23874, Doha, Qatar
[b] International Center for Chemical and Biological Sciences, HEJ Research Institute of Chemistry, University of Karachi, Karachi-75270, Pakistan
[c] Center of Hydrogen Energy, Institute of Future Energy, Universiti Teknologi Malaysia, Jalan Sultan Yahya Petra, 54100 Kuala Lumpur, Malaysia
[d] Malaysia-Japan International Institute of Technology, Universiti Teknologi Malaysia, Jalan Sultan Yahya Petra, 54100 Kuala Lumpur, Malaysia

ARTICLE INFO

Keywords:
Graphene Oxide
Polymeric Amine, Monomeric Amine, Cross-linking
OER

ABSTRACT

Practical applications of metal free catalysts are hindered by their innate poor stability for electrocatalytic application. Accordingly, in this study, synthesis and functionalization of graphene oxide via a modified Tour's method (GOT) with different amine containing molecules results in excellent catalytic performance and stability toward OER in alkaline medium. The as-synthesized polyethyleneimine GOT electrode (P-GOT), produced current densities of 10, 50 and 100 mA/cm^2 at overpotentials of 240, 350 and 420 mV, respectively, with small Tafel slope of 47 mV/dec. The X-ray diffraction analysis (XRD), Raman spectroscopy and X-ray photoelectron spectroscopy (XPS) analysis confirms the successful functionalization of GOT by ethylenediamine (E) and polyethyleneimine (P) molecules, respectively. Morphological studies based on field emission scanning electron microscopy (FESEM) confirm that the modification via covalent bonding preserved the original wrinkled and layered structure of GOT. **The** P-GOT with cross-linked amine can expose more active sites and is not easy to peel off, which corresponds to attaining lower charge transfer resistance (1.01Ω cm^2) and remarkable current stability in **1.0 M KOH** solution, compared to the pristine GOT and E-GOT electrodes. From this perspective, our results therefore provide a valuable route for development and practical application of metal free catalytic materials for water oxidation reaction.

Introduction

Clean energy has been one of the primary quests of the 21st century to substitute fossil fuels, which have been the main persistent energy source since the industrial revolution. Although fossil fuels have led to great industrial, economic, and social developments, it has been associated with very harsh environmental impacts, most significantly global warming and climate change [1–3]. The other main demerit with fossil fuels has recently been their high cost instability or price volatility, whereby costs can vary an order of magnitude over short time, hence propagating significant challenges to developed and developing economies [4, 5]. The development of renewable and sustainable energy resources to partially and gradually replace conventional fossil energy resources has been the main objective for many research efforts worldwide over the last few decades. Renewable energies such as solar, wind, tidal, geothermal, and hydro have been gradually developed and employed, presenting about 649 million tone oil equivalent (MTOE) in 2018 [6]. Hydrogen is considered the most sustainable and clean fuel, as the only fuel with zero-carbon emissions, since water is the only reaction product [7]. Hydrogen has been primarily sourced at large-scale process industries by reforming of fossil fuels, mostly natural gas and coal [8–10]. Sourcing hydrogen from vastly available water, more specifically seawater, through water electrolysis has been practiced for a long time, but has been mainly challenged by high energy consumption [11, 12]. Falling electricity costs from renewable solar PV or wind technologies is expected to make operational costs of water electrolysis much more favorable in the foreseeable future. Water electrolysis is a simple process in which electrical energy is utilized to split the water molecule into its two constituents, i.e., hydrogen and oxygen, according to the following simple reactions in alkaline media [13–15]:

* Corresponding authors.
E-mail addresses: zafarkhanghouri@hotmail.com, zafar_khan.ghouri@qatar.tamu.edu (Z.K. Ghouri), ahmed.abdel-wahab@qatar.tamu.edu (A. Abdel-Wahab).

https://doi.org/10.1016/j.mcat.2021.111960
Received 12 June 2021; Received in revised form 10 October 2021; Accepted 14 October 2021
Available online 31 October 2021

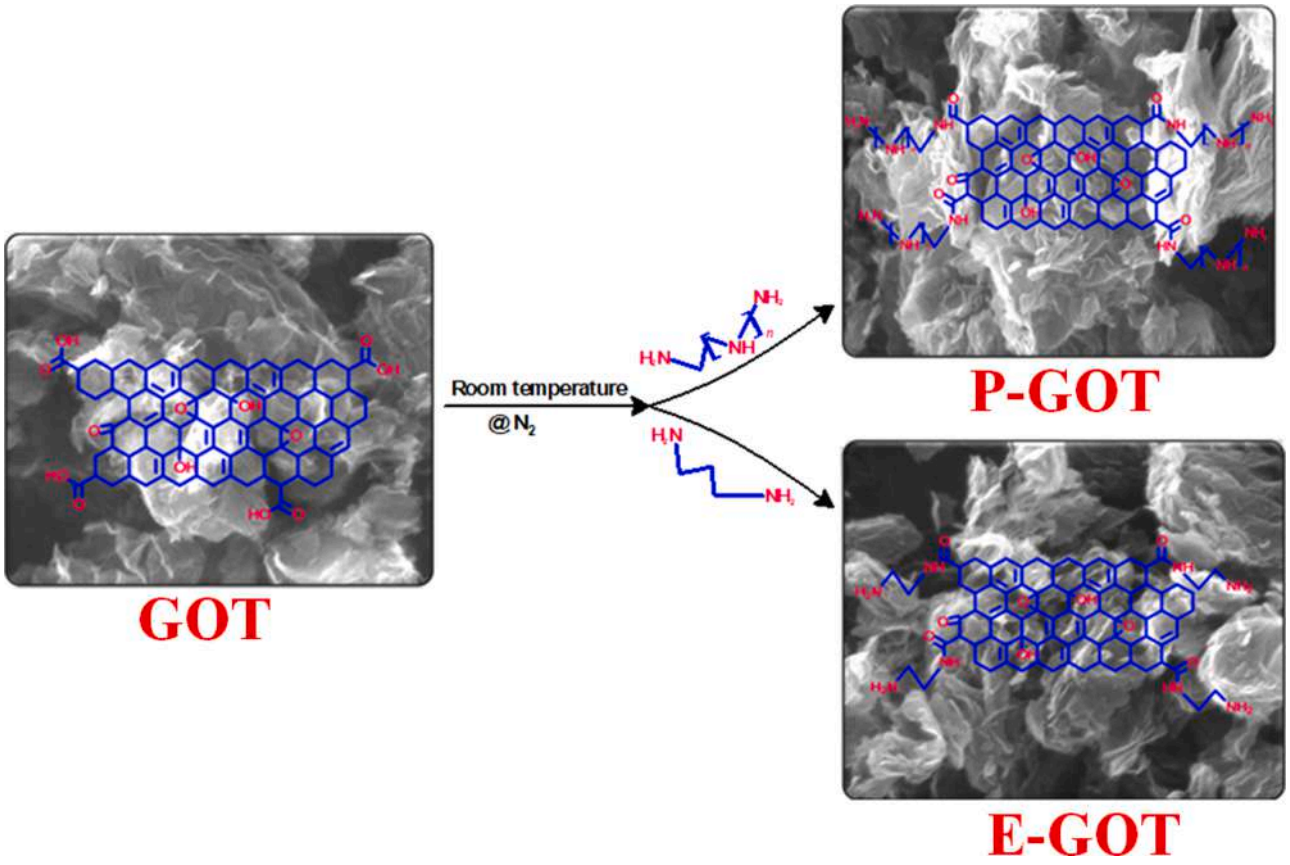

Scheme 1.. Schematic representation of the synthesis methods of ethylenediamine (E-GOT) and polyetyleneimine (P-GOT) functionalized graphene oxide.

Cathodic hydrogen evolution reaction HER: $2\ H_2O_{(l)} + 2\ e^- \rightarrow H_{2(g)} + 2\ OH^-$ (1)

Anodic oxygen evolution reaction OER: $2\ OH^- \rightarrow ½\ O_{2(g)} + H_2O_{(l)} + 2\ e^-$ (2)

Overall reaction water-splitting reaction: $H_2O_{(l)} \leftrightarrow H_{2(g)} + ½\ O_{2(g)}$ (3)

The reaction is catalyzed by electrocatalysts used as anodic and cathodic material, with noble metal such as platinum (Pt) and iridium or ruthenium oxides (IrO_2, RuO_2) being amongst the most effective for HER and OER, respectively, but with limited large scale application due to their high costs [16, 17]. Accordingly, different materials have been proposed and evaluated for efficient water electrolysis such as an array of transition metals [18–21] and carbon-based materials [22–25]. The efforts have been equally put to develop highly-efficient and low-cost electrodes for cathodic hydrogen evolution reaction (HER), and anodic oxygen evolution reaction (OER) [26–30]. Although both reactions are equally vital for the overall reaction to proceed, OER is more sluggish due to the need for involving the transfer of 4 electrons per O_2 molecule generation, as compared to the transfer of 2 electrons per H_2 molecule generation [31–33]. This in turn results in OER having much higher overpotentials, relative to the cathodic HER. Hence, extensive research efforts have been put into developing OER catalyst with high activity and stability from abundant and low-cost materials [34–36]. An interest have been devoted recently to develop and evaluate metal-free carbon-based electrocatalysts for OER as a promising functionalizable, efficient, and cost-effective materials, as this eliminates the requisite of incorporating precious metals [37, 38]. Graphene oxide, an oxidation product of graphite, has been shown to exhibit efficient electrochemical properties for many applications owing to its unique characteristics and most importantly ease of functionalization [39–41]. Since GO holds many oxygen containing functional groups, such as hydroxyl and epoxy groups on the basal plane and carboxyl groups at the edges [42], GO can be covalently functionalized in a facile manner by different organic molecules, such as aliphatic amines [43], amino acids [44], isocyanates and acyl chloride [45, 46]. Recently, tyramine functionalized graphene oxide (T-GO) have shown a low onset potential and Tafel slope of about 0.16 V and 69 mV/dec., respectively, with current density of about 2 mA/cm^2 [47]. Similarly, Lysine-functionalized GO have shown a low overpotential of 0.33 V at 10 mA/cm^2, but at higher Tafel slope of 80 mV/dec [48]. Unlike the reported complex steps for the functionalization of GO, in this work monomeric and polymeric amines were successfully grafted onto GOT nanosheet by a simpler single-step and inexpensive synthesis route. Specifically, the protocol for the reaction does not require heat and organic solvent, coupled with the advantage of attaining a high yield. Moreover, the surface chemistry, structure and morphology of the as-synthesized pristine GOT, **ethylenediamine functionalized graphene oxide (E-GOT) and polyethyleneimine functionalized graphene oxide (P-GOT)** has been well characterized by X-ray diffraction analysis (XRD), Raman spectroscopy, X-ray photoelectron spectroscopy (XPS) and scanning electron microscopy (SEM) techniques. The optimal P-GOT electrode exhibit superior electrocatalytic performance compared to those of pristine GOT and E-GOT toward OER in alkaline medium. Specifically, low OER overpotential of 240 mV at 10 mA cm^{-2} of current density **and** small Tafel slope (47 mV/dec.) indicating facile kinetics, and a remarkable stability.

Experimental

Chemicals

Graphite powder (GP), phosphoric acid (H_3PO_4), sulfuric acid (H_2SO_4), potassium permanganate ($KMnO_4$), hydrogen peroxide (H_2O_2), potassium hydroxide (KOH) and ethanol (C_2H_5OH) were purchased and used without any further purification. Ethylenediamine (E) (99.5%), polyethyleneimine (P; Mw 10,000) was purchased from Sigma-Aldrich while deionized (DI) water were used for all syntheses.

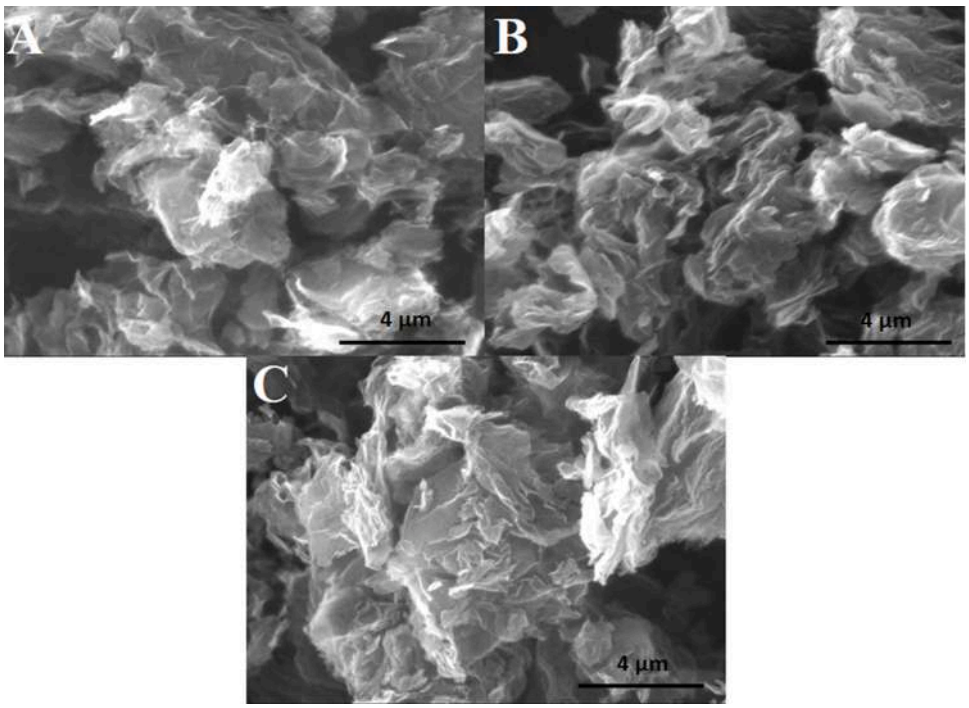

Fig. 1. SEM images for prepared (A) pristine GOT (B) E-GOT and (C) P-GOT powder.

GO synthesis

Graphene Oxide (GOT) was synthesized from graphite powder (GP) by a modified Tour's method [49]. In a typical synthesis, mixed acid solution was first prepared (360 mL H_2SO_4 and 40 ml of H_3PO_4) and added to the mixture of graphite powder and $KMnO_4$, then heated to 50°−60° C for 12 h. **After that, the mixture was cooled down by adding 400 mL of ice cubes, followed by 3 mL of 30% H_2O_2 added drop-wise, while reaction temperature was maintained between 18°−20° C.** The obtained suspension was then filtered and washed with deionized water and ethanol several times to remove free ions and dried to obtain GOT powder.

Amine-Functionalization

For functionalization, the first 250 mg of the above-synthesized GOT was dispersed in 200 ml deionized water and then probe-sonicated for 5 min at 2 s ON / 3 s OFF pulsing by the addition of a specific amount of ethylenediamine/polyethyleneimine. **After that, the mixture was sonicated for an additional 10 min and left to react overnight under slow stirring in an inert atmosphere at ambient temperature.** The resulting suspension was then washed to remove unbounded ethylenediamine /polyethyleneimine and finally collected by vacuum filtration **(**Scheme 1**).**

Materials characterization

Powder X-ray diffraction (XRD) data were collected to analyze the crystal structure and stacking of **GOT, E-GOT and P-GOT** using Ultima IV X-ray diffractometer with Cu-α radiation (λ = 0.154148 nm operating at 40 kV and 20 mA in step scan mode, between 2°θ to 40°θ while the interlayer d-spacing was calculated from Bragg's Law. Raman data were obtained to study the effect of functionalization on the order/disorder structure of GOT, E-GOT and P-GOT by Raman spectroscopy (DXR Dispersive Raman, Thermo Fisher Sci.). The surface chemistry of GOT, E-GOT and P-GOT were analyzed by **Fourier transform infrared spectroscopy (FTIR, Bruker Vertex 70) and** X-ray photoelectron spectroscopy (XPS) (Escalab 250 Xi, Thermo Fisher Sci.) with 20 eV pass energy for high-resolution scans and 100 eV for survey scans. The surface morphology was analyzed using a scanning electron microscope (SEM).

Electrode preparation

The active area of stationary glassy carbon electrode (GCE) was first cleaned with isopropanol and polished with diamond suspension. The polished GCE was then sonicated with DI water for 10 min to remove the traces of diamond suspension. 2.0 mg of the GOT/E-GOT /P-GOT powder was ultrasonically dispersed in a suspension of 200μL n-propanol, 200 μL DI water and 25 μL of Nafion 117 solution. 15 μL of the prepared suspension was then drop-casted onto the active GCE area and dried at 80 °C for 30 min.

Electrochemical measurements

All electrochemical measurements (cyclic voltammetry, linear sweep voltammetry, chronoamperometry and electrochemical impedance spectroscopy) were performed on an electrochemical workstation, Reference 3000 potentiostat (Gamry, PA, USA) at room temperature in 1.0 M KOH aqueous solution. Platinum wire and Ag/AgCl (saturated in KCl solution) electrode were used as a counter and reference electrode, respectively. All potentials were measured with respect to Ag/AgCl and normalized to reversible hydrogen electrode (RHE) according to Nernst equation: E (RHE) = E (Ag/AgCl) + (0.059 pH) + 0.197 V.

Results and discussions

Physicochemical studies

The surface morphology of pristine and functionalized graphene oxide were investigated by SEM image analysis. The SEM image of pristine GOT in Fig. 1(A), shows the typical wrinkled morphology while the dark and light areas show layered structure of GOT. It is worth noting that the images of E-GOT and P-GOT in Fig. 1 (B and C) showed morphology that is quite similar to pristine GOT, which suggested that the modification via covalent bonding preserved the original wrinkled and layered structure of GOT. Although the pristine and modified GOT have similar structure, the darker color and more wrinkled in modified GOT could be due to the amination [50, 51]. Further, the XRD patterns of GOT, E-GOT and P-GOT electrodes are shown in Fig. 2(A), where the

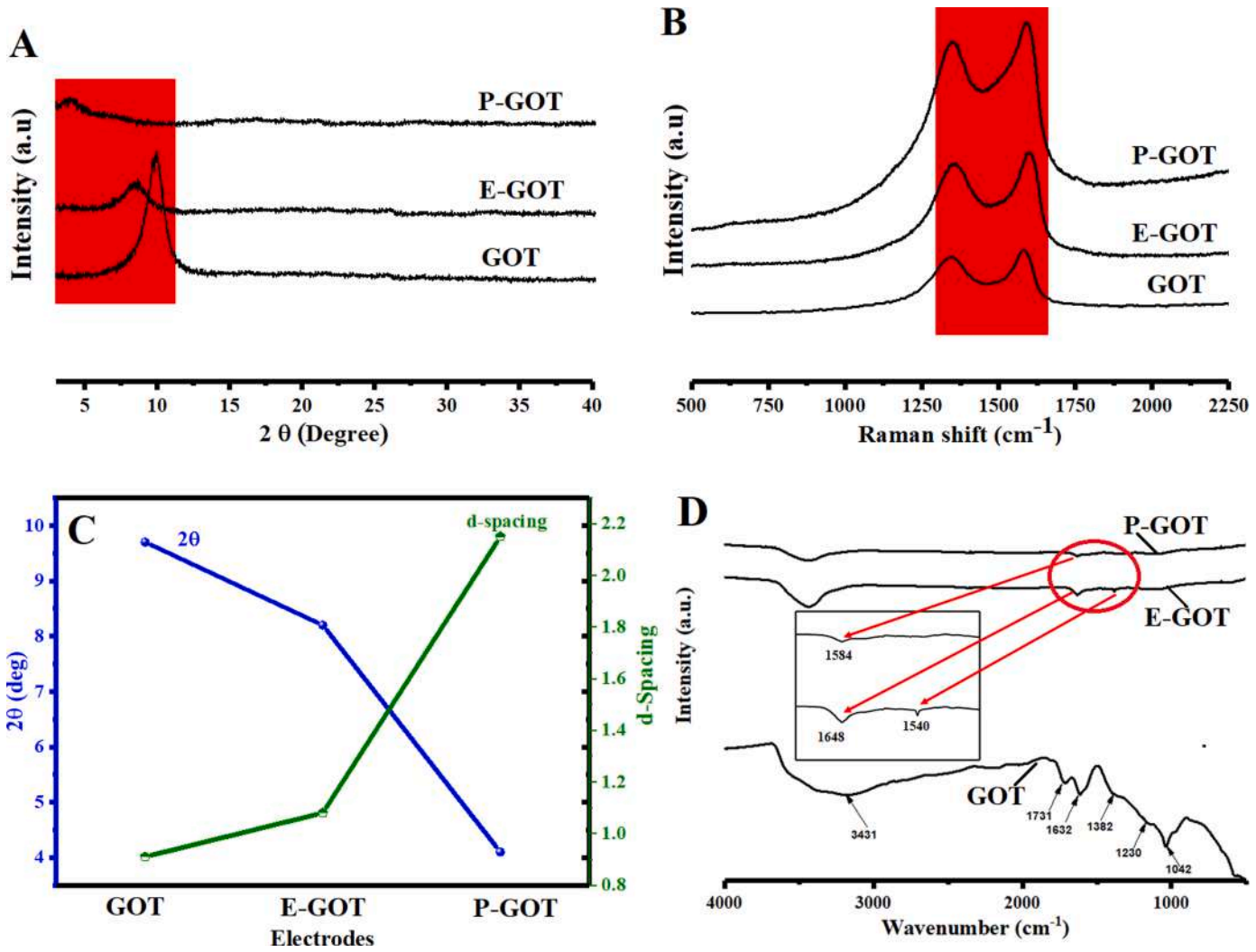

Fig. 2. (A) XRD patterns, (B) Raman spectra, (C) diffraction angle and D-spacing and (D) FTIR spectra for prepared pristine GOT, E-GOT and P-GOT powder. The inset image shows high magnification for the marked area.

oxidation of graphite by the modified Tour method was confirmed by the standard diffraction peak located at 2θ value of 10° corresponded to the d_{001} crystal plane [52], which indicates the presence of oxygen rich functional groups [53, 54]. A slight shift of (002) carbon representative peak toward lower diffraction angle (2θ=8.2) and higher d-spacing (1.08 nm) for E-GOT electrode can be associated with the introduction of ethylenediamine monomer (Fig. 2 (A&C)). On the other hand a sharp shift of (002) carbon representative peak from 2 value of 10° to 4.1° for P-GOT can be associated with insertion of polyethyleneimine macromolecule into the GOT laminates. The increase in the d-spacing of P-GOT could possibly be due to larger steric hindrances effect of the polymer/GOT interaction (Fig. 2(C)). The structural characteristics of pristine GOT, E-GOT and P-GOT electrodes were further analyzed by Raman spectroscopy, as presented by the spectra shown in Fig. 2(B). Typically, Raman spectra for all the electrodes exhibited two distinct bands, namely a D-band located at ~1358 cm^{-1} **originated from a second order scattering due to the A1g in-plane breathing vibrational modes of Sp2 rings and reflects the inherent defects and edge effects of graphene microcrystals and G-band located at 1590 cm^{-1} attributed to the first order scattering of the E2g in-plane vibration mode of Sp2 graphitic carbon atoms [55]. It is well known that the relative band intensity ratio of D and G (I_D/I_G) reflects the disorder caused by lattice defect of graphene structure [56]. The controlled functionalization of GO introduced defects in structure of GO and decreased its graphitization, as indicated the intensity ratios of D band to the G band of E-GOT (0.94) and P-GOT (0.95) were comparatively higher than that of pristine GOT (0.92), which suggested that defects originated from effective grafting of amines groups of ethylenediamine/polyethyleneimine in the GOT framework.**

The functional groups of pristine GOT, E-GOT, and P-GOT were characterized by FT-IR (Fig. 2(D)). The characteristic peaks of pristine GOT shows the presence of carboxyl groups (C=;O andC—OH) at 1730 and 1632 cm^{-1}, stretching vibration of epoxy groups (C—O) at 1230 and 1042 cm^{-1}, and the hydroxyl groups at 3431 cm^{-1}, respectively [57]. After modification with EDA, the characteristic peaks ofC=O and C—OH groups were disappeared, while two new peaks representing the amide-I and amide-II bond were observed at around 1650 and 1540 cm^{-1}, respectively while, a new amide-I bond at 1584 cm^{-1} was observed after the modification with PEI (marked by red arrows along with high magnification). The vanish and generation of new bonds show that the amine group of EDA and PEI possibly reacted with carboxyl groups (C= O and C—OH) and formed amide group.

Furthermore, the surface chemistry and chemical compositions of pristine GOT, E-GOT, and P-GOT electrode were investigated by XPS analysis. As seen in the full survey spectrum of **pristine** GOT only two peaks located at 284.8 and 531.9 eV are present and they

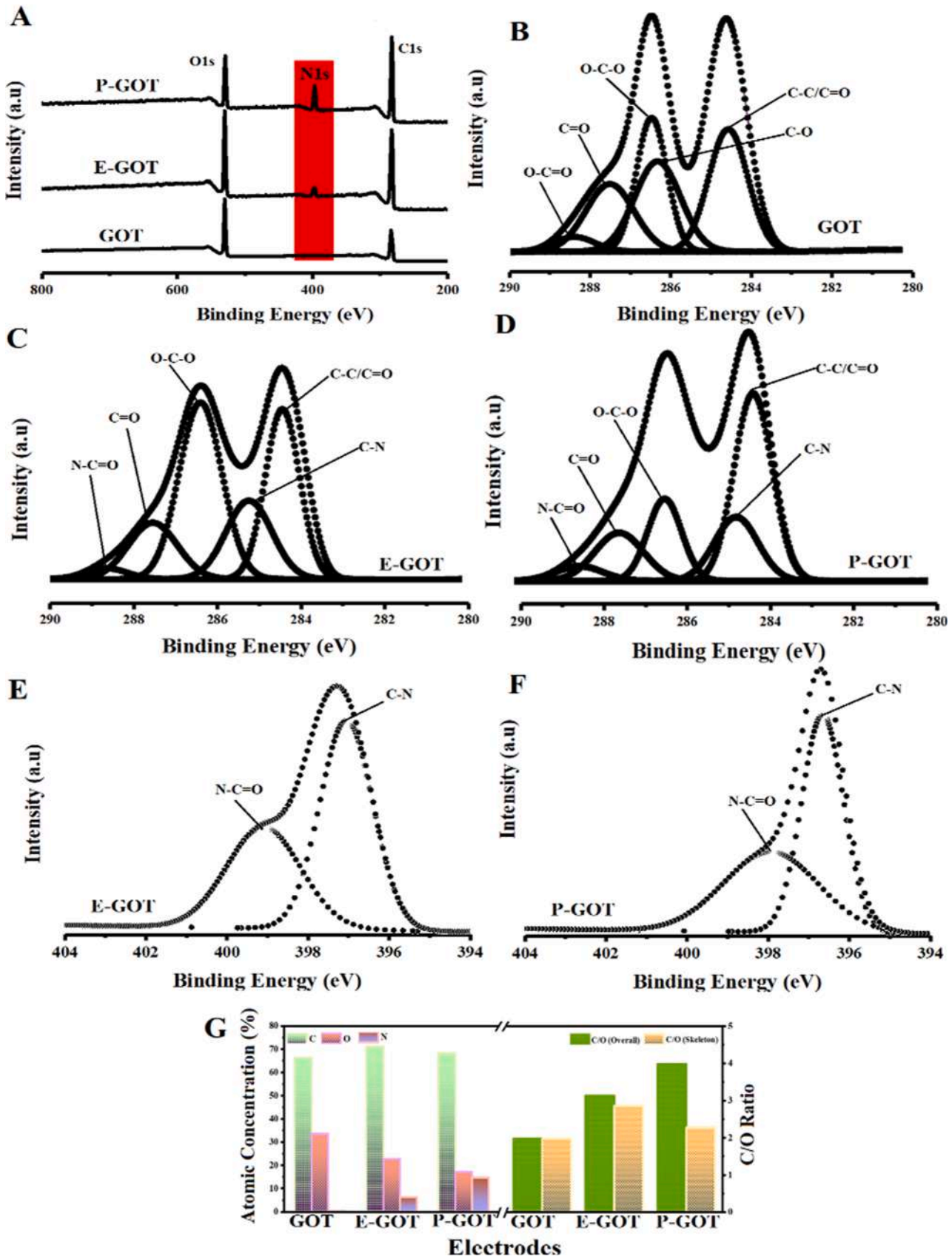

Fig. 3. (A) Full scan XPS (B), C1s spectra of pristine GOT, (C) C1s spectra of E-GOT, (D) C1s spectra of P-GOT, (E) N1s spectra of E-GOT, (F) N1s spectra of P-GOT and (D) elemental composition for prepared pristine GOT, E-GOT and P-GOT powder.

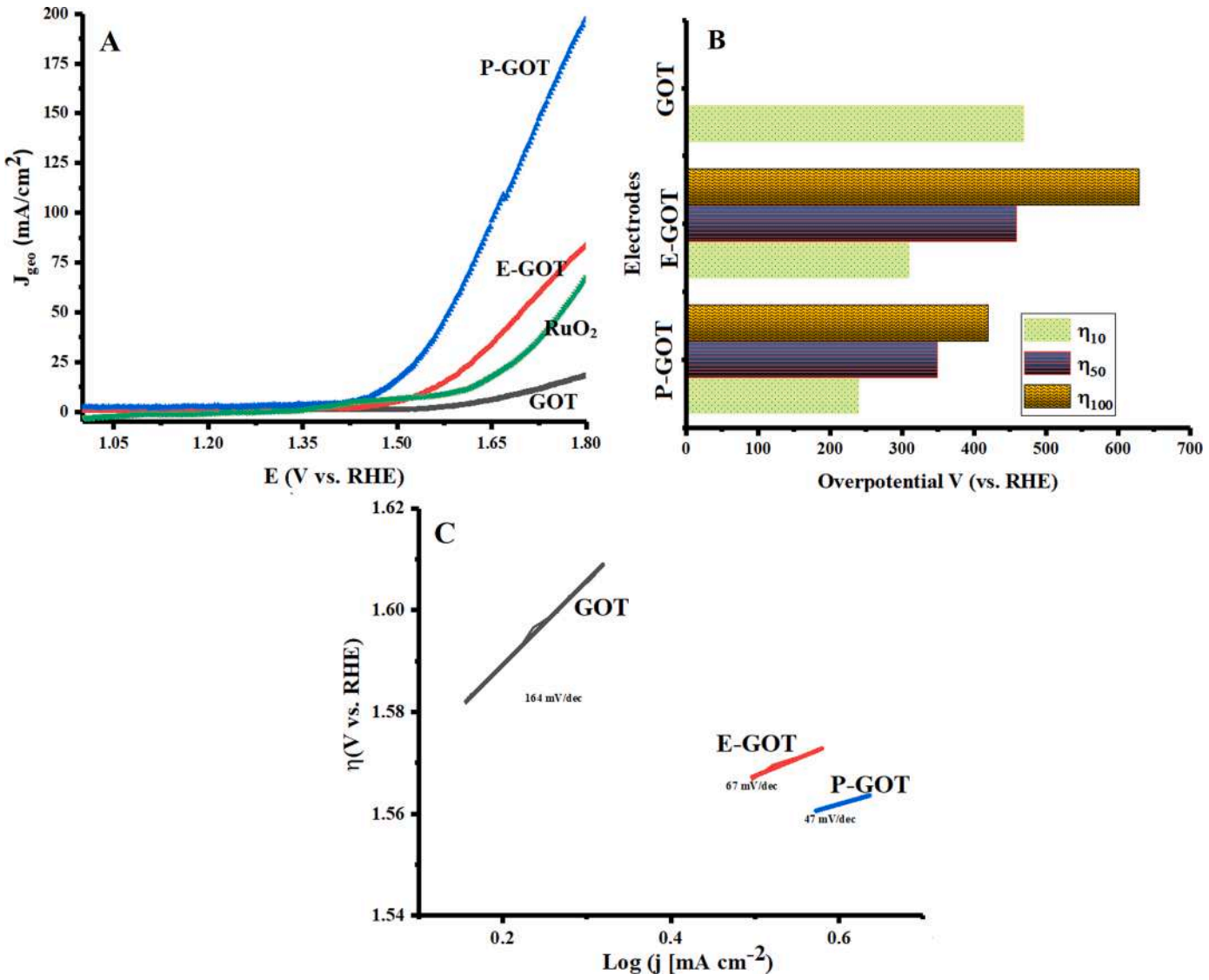

Fig. 4. (A) OER measurements in 1 M KOH recorded at a scan rate of 10 mVs^{-1} (B) Over-potential to reached the current density of 10, 50 and 100 $mAcm^{-2}$ and (C) Tafel plot for prepared pristine GOT, E-GOT and P-GOT electrode.

correspond to C1s and O1s, respectively **(Fig. 3(A)).** Clearly, the full survey spectrum of E-GOT and P-GOT, shows a new peak at 399 eV, corresponding to the N1s along with the common signals corresponding to C1s and O1s **(Fig. 3(A)). The high-resolution C1s spectra of pristine GOT shows five characteristic peaks at ≈ 284.6, 286.3, 286.9, 287.2 and 288.5 eV corresponding to theC—C/C=>C, C—O, C—O-C, C = O and O—C = O species, respectively (Fig. 3(B)). As shown in the Fig. 3 (C-D), after modification by EDA and PEI, two new peaks appeared at 285.6 and 288.7 eV which are assigned to the binding energy of C—N and N—C=O species, respectively. According to the high-resolution N1s spectra of E-GOT and P-GOT (Fig. 3 (E and F)), there are two types of nitrogen groups located at ~398.8 and ~399.9 eV attributed to the pyridinic-N and amine-N groups.** [58-61]. **Obviously, the N1s spectra of E-GOT (Fig. 3(E)) show a weakened peak of C—N compared to the N1s spectra of P-GOT ((Fig. 3(F)). According to (Fig. 3(G)),** nitrogen atomic percentage is maximum in P-GOT and minimum in E-GOT, while the oxygen atomic-concentration dramatically decreased and the carbon to oxygen ratio of E-GOT and P-GOT significantly increased compared to GOT **(Fig. 3(G)).** Accordingly, these observations clearly indicate that the anchoring sides of **pristine** GOT was successfully functionalized with ethylenediamine/polyethyleneimine, molecules. **However, XPS results indicates the formation of new covalent bonds of C—N and N—C=O, which further evident that ethylenediamine and polyethyleneimine molecules successfully grafted onto GOT laminates via the formation of amide groups.**

Electrochemical studies toward OER

The oxygen evolution reaction (OER) is an energy intensive multi-step process in water splitting and requires a large overpotential (OER, $4H^{+}/4e^{-}$) [62–64]. In addition, it is well known that OER activity mainly depends on electrolyte solution. In fact, changes in the alkaline electrolyte concentration influenced the current density but do not have significant impact on the onset potential [65, 66].

Consequently, the electrocatalytic OER activity of pristine GOT, E-GOT and P-GOT were evaluated along with RuO_2 (for comparison purpose) in 1.0 M KOH solution by using linear sweep voltammetry (LSV) technique with the potential range of 1.0 to 1.8 V (vs. RHE). It is also worth mentioning that the presence of metallic contaminations (i.e., nickel and iron) in graphene are ubiquitous, originating from starting material (graphite powder) and significantly influencing their catalytic properties [67, 68]. Therefore, elemental analyses on pristine GOT, E-GOT, and P-GOT were

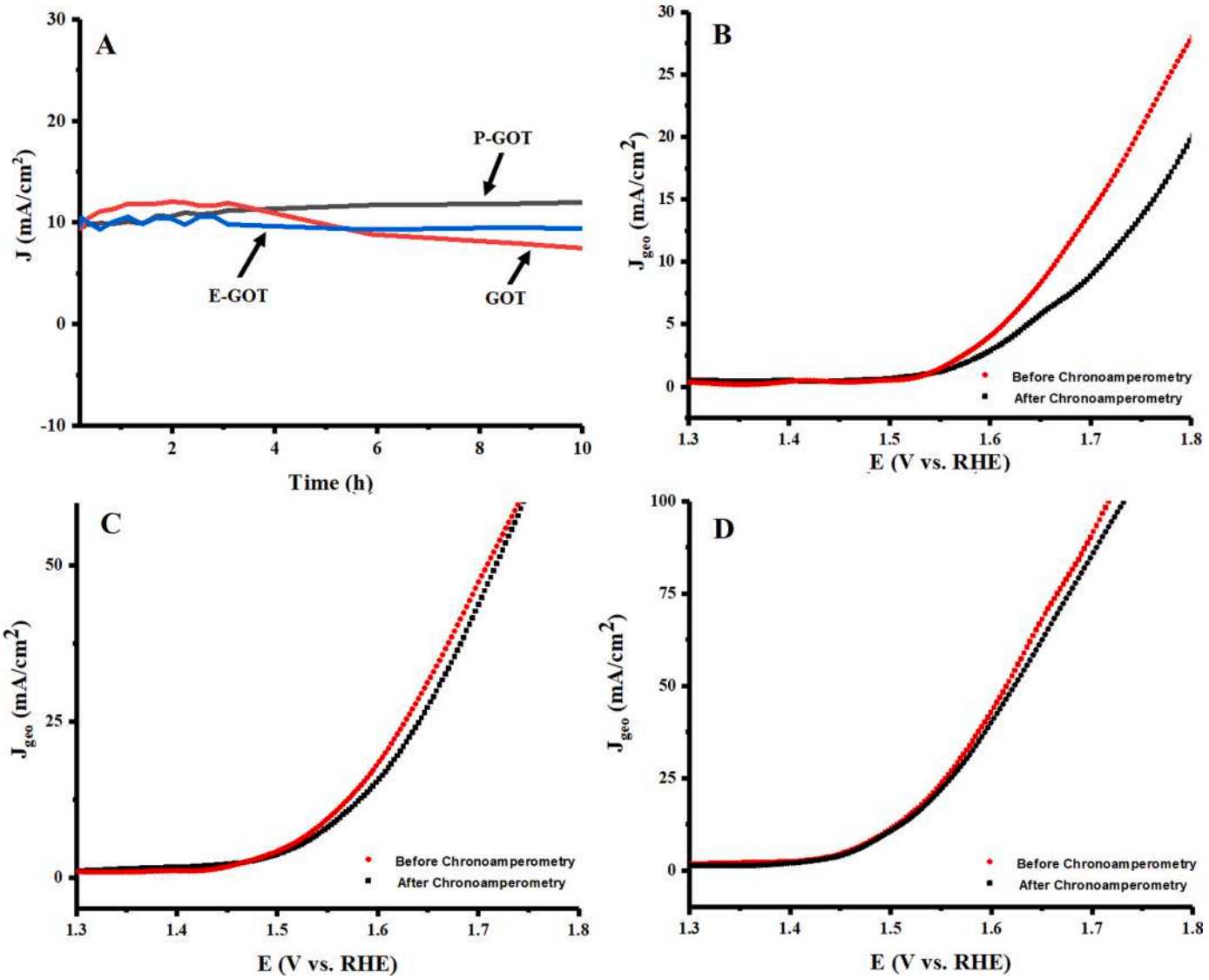

Fig. 5. (A) Chronoamperometry measurements and (C-D) Deviation in over potential after 10 h chronoamperometry measurements for **pristine** GOT, E-GOT and P-GOT electrode, respectively.

performed using the ICP-MS technique before the electrochemical investigations. It can be seen in (SI Table.1.) that both the GOT (unfunctionalized and functionalized) samples, as expected, contains traces of metals include Fe, Co, Cu, Ni, Mo, and Mn, with the existence of Fe as most abundant element. Further, it can be observed that both the GOT (unfunctionalized and functionalized) showed quite similar metal contaminations for all the elements, which suggest that the modification via covalent bonding did not have substantial impact on metallic contaminations. However, comparative OER polarization curve in Fig. 4**(A)** shows that P-GOT electrode exhibited an optimal current response toward OER with early onset potential (85 mV) compared to the E-GOT (92 mV) and **pristine** GOT (110 mV). Interestingly, **E-GOT** and P-GOT electrode's OER current response and overpotential (η) is even comparable to the state-of-art RuO_2 (Fig. 4**(A))** [69]. The OER current density response of the **pristine** GOT recorded at η =370 mV vs. RHE (1.6 V) at a current density of ~3.5 mA/cm^2. However, the E-GOT and P-GOT electrodes displayed significantly high OER current density response of 20 and 50 mA/cm^2, respectively, at the same η values of 370 mV vs. RHE (1.6 V). Moreover, to reach the current density of 10, 50 and 100 mA/cm^2, the P-GOT requires overpotentials of 240, 350 and 420 mV, respectively, which are significantly lower than that of E-GOT (310, 460 and 630 mV) (Fig. 4 **(B))**. The observed overpotential value for P-GOT (240mV@10 mA/cm^2) is much lower than many reported metal-free OER catalysts such as N,S-CNT (360 mV) [70], ONPPGC/OCC (410 mV) [71], NFPGN (340 mV) [72], GO-PANi-FP (520 mV) [73] and Ly-rGO (330 mV)[48] as shown in Fig. 7**(A)**. Further, P-GOT required an overpotential lower than those of previously reported **carbon-metals based systems** such as Co_3O_4/NPC (270 mV) [74], Ni@NC (280 mV) [75], Co-Gr (350 mV) [76], CoP/N,P-Gr (270 mV) [77] and FeN_4/CF/EG (290 mV) [78] as shown in Fig. 7**(B)**. On the other hand, **pristine** GOT electrode deliver the current density of only 10 mA/cm^2 within the same tested potential range **(**Fig. 4**(B))**.

The Tafel slope derived from LSV curve is an important parameter used for revealing the inherent kinetics of the electrode and can elucidate the rate determining step involved in the catalytic reactions [79]. The linear regions of the Tafel slope were fitted by Tafel equation (η = blog (j/j_0), where η is the overpotential, b is the Tafel slope, j is the current density, and j_0 is the exchange current density. Accordingly, Fig. 4**(C)** reveals smaller Tafel slope of 47 mV/dec for P-GOT relative to E-GOT (67 mV dec^{-1}) and **pristine** GOT (164 mV dec^{-1}). These results further demonstrate better intrinsic OER kinetics of the P-GOT contrary to its **pristine** GOT counterparts. The catalytic stability is an important parameter for anodic materials in water oxidation technology.

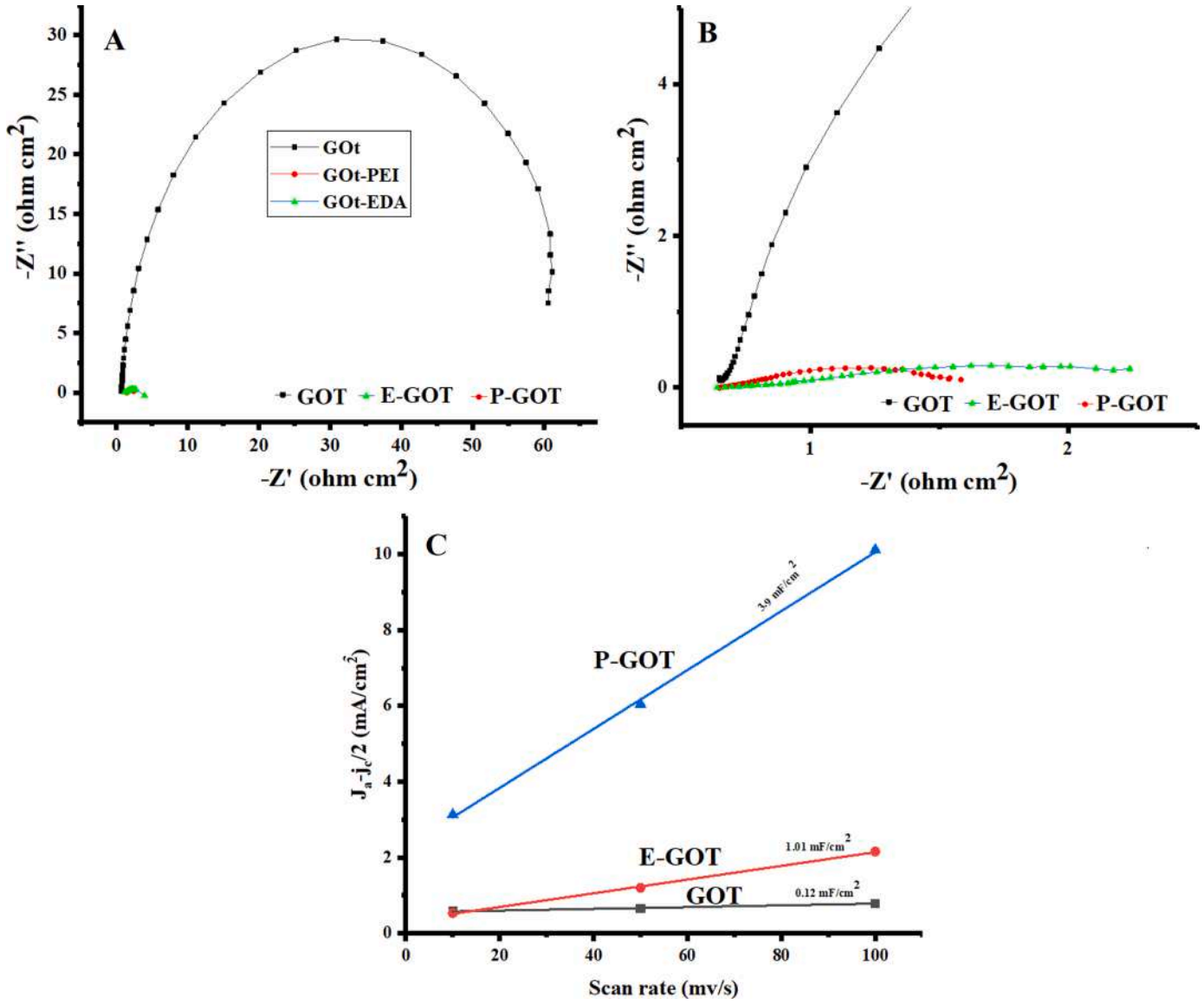

Fig. 6. (A) EIS, (B) high magnification EIS image and (C) Electrochemical surface areas (ECSA) for prepared pristine GOT, E-GOT and P-GOT electrode.

Typically, the practical application of metal free catalysts is hindered by their poor stability. Therefore, to check the long term stability of the **pristine** GOT, E-GOT and P-GOT electrodes toward OER, the electrocatalysts were examined by the chronoamperometric (CA) technique at a constant potential vs. RHE for over 10 h in 1.0 M KOH solution and the results are shown in Fig. 5**(A))**. As seen, **pristine** GOT electrode showed considerable decrease in the attained OER current density. On the other hand, E-GOT and P-GOT electrodes showed stable current density response with no significant change after 10 h of CA operation. In addition, **(**Fig. 5 **(B-D))** shows the OER polarization curves before and after CA measurements. As seen, there was a significant change towards the requirement of higher overpotentials after 10 h CA measurements for both **pristine** GOT and E-GOT electrodes, relative to the initial overpotential before CA **(**Fig. 5 **(B-C))**. Notably, the overpotential for P-GOT electrode was only increased by 4 mV after 10 h of CA measurements **(**Fig. 5**(D)). Moreover, after 10 h chronoamperometric test, no significant change in morphology of P-GOT was observed (supporting information, Figure S2).** We consider that the GOT cross-linked with amine have a strong bond to the electrode, which endows the catalyst with excellent stability and durability. In order to understand the reason behind the improved catalytic performance of P-GOT toward OER, the electrochemical active surface area (ECSA) of three electrodes (**pristine** GOT, E-GOT and P-GOT) can be compared through the double-layer capacitance (C_{dl}) values measured from the CV curve within a non-faradic narrow potential window. Normally, the double-layer capacitance represents the ECSA and extracted by plotting the $\Delta j = (J_a - J_c)$ against the scan rates [80]. Therefore, to measure the electrochemical double layer capacitance, CV measurements were performed under increasing scan rates. As shown in Fig. 6**(C),** the electrochemical double layer capacitance values obtained from the CV curves **(supporting information, Figure S1)** for P-GOT is 3.9 mF/cm^2, which is almost 4 and 32 times larger than E-GOT and **pristine** GOT, respectively. The ECSA results are consistent with the OER activity **(**Fig. 4**(A))** as high active surface area often lead to improve the catalytic activity [81]. Therefore, the improved OER activity of P-GOT may be in part due to the large ECSA.

In order to gain more insights into the improved catalytic activity of P-GOT, electrochemical independence spectroscopy (EIS) of **pristine** GOT, E-GOT and P-GOT under the OER reaction conditions were performed and the results are presented in Fig. 6**(A&B)** and summarized in Table 1. The recorded charge-transfer resistance (R_{ct}) value of P-GOT (1.01Ωcm^2) is much smaller than E-GOT (2.13 Ωcm^2) and **pristine** GOT

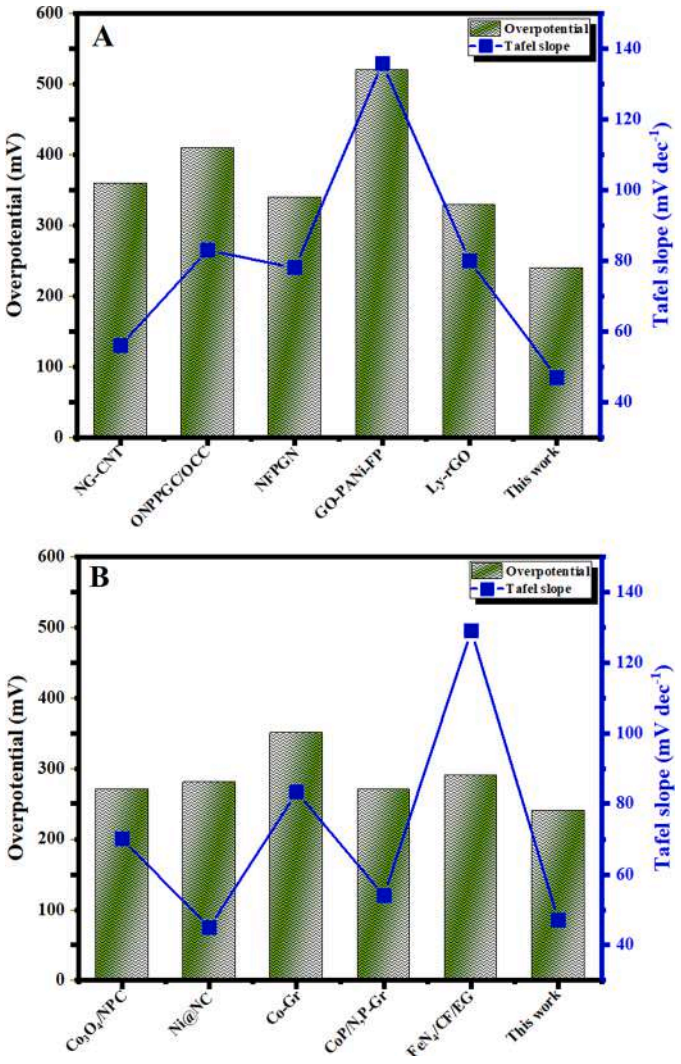

Fig. 7.. Comparative study for P-GOT versus (A) metal free electrocatalyst and (B) metal based electrocatalyst toward oxyen evolation reaction in 1.0 M KOH solutions.

(47.11 Ωcm^2), suggesting an enhanced charge transport upon incorporation of cross-linked amine groups. Interestingly, this finding is consistent with the results of current density, Tafel slopes and ECSA (**Figs. 4 and 6**).

Remarkable improved OER activity of P-GOT might be directly correlated with decreased charge transport resistance and increased ECSA. However, based on these results, we surmised that the overall activities of P-GOT might be attributed to the strong electronic interaction at GOT and polymeric amine interfaces, which are highly beneficial for electrocatalytic active sites. In addition, the modified electronic structure of the GOT by cross-linked polymeric amine molecule could introduced extra electrons to boost O_2 adsorption on GOT surface. Further, the polymeric amine functionalities break the electroneutrality of sp_2 carbon atom of graphene oxide, which could activate the π electrons of carbon, in turn activating P-GOT towards more efficient OER. **We assume that the GOT cross-linked with polymeric amine can create electron rich or deficient sites. These sites could be responsible for abundant defective edges, which favorably provides multidimensional electron transport pathways toward the OER. The** GOT cross-linked by monomeric amine can efficiently enhance the catalytic activity of E-GOT towards OER. **The intensity ratios of D band to the G band of GO-PEI (0.95) showed highly defective structure, which might alter atomic orbital and generate localized electronic states that could also be associated with higher OER activity** [82].

It is well-known that the OER mechanism over the metal-free electrocatalysts are more complex than the metallic electrocatalyst. However, based on the experimental data, the possible mechanistic path for OER over the modified electrode could be as follows:

The OER reaction was first, initiated by adsorption of hydroxide ion (OH^-) from the water on the active site of $(P-GOT)$ followed by the removal of an electron, which results in formation of $(P-GOT)OH^*_{abs}$ via the following reaction:

$$(P-GOT)+OH^- \rightarrow (P-GOT)OH^*_{abs}+e^- \quad (4)$$

Further, $(P-GOT)OH^*_{abs}$ is converted to $(P-GOT)O^-$ species by simultaneous removal of proton and an electron via the following reaction:

$$(P-GOT)OH^*_{abs}+OH^- \rightarrow (P-GOT)O^-+H_2O+e^- \quad (5)$$

Whereas, OH^- combines with $(P-GOT)O^-$ to form the hydroperoxide intermediate $(P-GOT)OOH$ via the following reaction:

$$(P-GOT)O^-+OH^- \rightarrow (P-GOT)OOH+e^- \quad (6)$$

Finally, OH^- can react with $(P-GOT)OOH$ intermediate and generate O_2 molecule via the following reaction:

$$(P-GOT)OOH+\ OH^- \rightarrow (P-GOT)+\ O_2+H_2O+e^- \quad (7)$$

The above-mentioned mechanistic pathway for the electron transfer is in good agreement with previous work [83–91].

Conclusion

Typically, stability is the main dilemma facing the metal-free electrocatalysts, as most of the metal-free materials dissolve in reaction media of interest for OER. Accordingly, we demonstrated that the GOT sheets cross-linked with amine could have a strong bond to the electrode, which endows the catalyst with excellent performance and stability in an alkaline medium. Amine groups were successfully pillared between GOT nanosheets by a simple one-step solvent-free amination technique. The obtained data demonstrates that the modified GOT (P-GOT) is highly active toward OER in alkaline medium, as low overpotentials of 240, 350, and 420 mV are required to achieve current densities of 10, 50, and 100 mA cm^{-2}, respectively, with a Tafel slope of 47 mV/dec. Also, the P-GOT electrode exhibit remarkable stability for 10 h of chronoamperometric operation. **Although the effect of metallic contamination on the electrochemical properties of GO cannot be rule out, we attributed the main electrolytic response to the role of amine groups.** This performance is superior to most of the reported metal free catalyst for OER reaction. The obtained data demonstrate that the fabricated electrode could be a promising and cost-effective candidate for practical application upon further optimization

Table 1.
Summary of information over various catalysts.

Catalysts	Onset Potential (V)	η@10 (mA/cm^2)	η@50 (mA/cm^2)	η@100 (mA/cm^2)	Tafel slope (mV/dec.)	ECSA	Rct Ωcm^2
GOT	1.10	470	–	–	164	0.12	47.11
E-GOT	0.92	310	460	630	67	1.01	2.13
P-GOT	0.85	240	350	420	47	3.90	1.01

of the materials.

Credit author statement

Z.K.G: Conceptualization, Methodology, Investigation, Data Curation, Formal analysis, Visualization, Writing, Original draft preparation, Review and Editing; **K.E:** Formal analysis, Writing, Review and Editing; **A.B:** Formal analysis and Review; **N.W.J:** Data Curation and Formal analysis; **M.N:** Validation, Formal analysis, Review and Editing; **A.A:** Funding acquisition, Validation, Writing, Review and Editing.

Declaration of Competing Interest

The authors declare that they have no known competing financial interests or personal relationships that could have appeared to influence the work reported in this paper.

Acknowledgement

This study is supported by a grant from the Qatar National Research Fund under National Priorities Research Program – Award Number – NPRP12S-0131–190024 and co-funding support from Qatar Shell Research and Technology Center (QSRTC). The paper's contents are solely the responsibility of the authors and do not necessarily represent the official views of the Qatar National Research Fund. Further, Zafar Khan Ghouri and M.M. Nasef wish to acknowledge Research Fellow Grant from Ministry of Higher Education through Universiti Teknologi Malaysia with Q.K130000.21A6.00P22.

Supplementary materials

Supplementary material associated with this article can be found, in the online version, at doi:10.1016/j.mcat.2021.111960.

References

[1] X. Zhou, C. Feng, The impact of environmental regulation on fossil energy consumption in China: direct and indirect effects, J. Clean. Prod. 142 (2017) 3174–3183.
[2] S.A. Solarin, An environmental impact assessment of fossil fuel subsidies in emerging and developing economies, Environ. Impact Assess. Rev. 85 (2020), 106443.
[3] C. Gaete-Morales, A. Gallego-Schmid, L. Stamford, A. Azapagic, Life cycle environmental impacts of electricity from fossil fuels in Chile over a ten-year period, J. Clean. Prod. 232 (2019) 1499–1512.
[4] C. García-Martos, J. Rodríguez, M.J. Sánchez, Modelling and forecasting fossil fuels, CO2 and electricity prices and their volatilities, Appl. Energy 101 (2013) 363–375.
[5] Z.-.M. Chen, P.-.L. Chen, Z. Ma, S. Xu, T. Hayat, A. Alsaedi, Inflationary and distributional effects of fossil energy price fluctuation on the Chinese economy, Energy 187 (2019), 115974.
[6] Total Energy Supply (TES) By Source 2021, International Energy Association.
[7] H. Caliskan, I. Dincer, A. Hepbasli, Exergoeconomic and environmental impact analyses of a renewable energy based hydrogen production system, Int. J. Hydrog. Energy 38 (2013) 6104–6111.
[8] G. Iaquaniello, F. Giacobbe, B. Morico, S. Cosenza, A. Farace, Membrane reforming in converting natural gas to hydrogen: production costs, Part II, Int. J. Hydrog. Energy 33 (2008) 6595–6601.
[9] H.C. Yoon, P.A. Erickson, Hydrogen from coal-derived methanol via autothermal reforming processes, Int. J. Hydrog. Energy 33 (2008) 57–63.
[10] T.A. Adams II, P.I. Barton, Combining coal gasification and natural gas reforming for efficient polygeneration, Fuel Process. Tech. 92 (2011) 639–655.
[11] A. Ursua, L.M. Gandia, P. Sanchis, Hydrogen production from water electrolysis: current status and future trends, Proc. IEEE 100 (2011) 410–426.
[12] P. Millet, S. Grigoriev, L. Diéguez, Renewable Hydrogen Technologies, Production, Purification, Storage, Applications and Safety, (2013) 19–40.
[13] M. David, C. Ocampo-Martínez, R. Sánchez-Peña, Advances in alkaline water electrolyzers: a review, J. Energy Storage 23 (2019) 392–403.
[14] J. Lamb, C.J. Orendorff, L.A.M. Steele, S.W. Spangler, Failure propagation in multi-cell lithium ion batteries, J. Power Sources 283 (2015) 517–523.
[15] C. Lamy, From hydrogen production by water electrolysis to its utilization in a PEM fuel cell or in a SO fuel cell: some considerations on the energy efficiencies, Int. J. Hydrog. Energy 41 (2016) 15415–15425.
[16] S. Dresp, F. Dionigi, S. Loos, J. Ferreira de Araujo, C. Spöri, M. Gliech, H. Dau, P. Strasser, Direct electrolytic splitting of seawater: activity, selectivity, degradation, and recovery studied from the molecular catalyst structure to the electrolyzer cell level, Adv. Energy Mater. 8 (2018), 1800338.
[17] Z. Kang, S.M. Alia, J.L. Young, G. Bender, Effects of various parameters of different porous transport layers in proton exchange membrane water electrolysis, Electrochim. Acta 354 (2020), 136641.
[18] W.-.F. Chen, J.T. Muckerman, E. Fujita, Recent developments in transition metal carbides and nitrides as hydrogen evolution electrocatalysts, Chem. Commun. 49 (2013) 8896–8909.
[19] B.M. Tackett, W. Sheng, J.G. Chen, Opportunities and challenges in utilizing metal-modified transition metal carbides as low-cost electrocatalysts, Joule (1) (2017) 253–263.
[20] M.A. Ahsan, A.R. Puente Santiago, Y. Hong, N. Zhang, M. Cano, E. Rodriguez-Castellon, L. Echegoyen, S.T. Sreenivasan, J.C. Noveron, Tuning of trifunctional NiCu bimetallic nanoparticles confined in a porous carbon network with surface composition and local structural distortions for the electrocatalytic oxygen reduction, oxygen and hydrogen evolution reactions, J. Am. Chem. Soc. 142 (2020) 14688–14701.
[21] M.F. Sanad, A.R. Puente Santiago, S.A. Tolba, M.A. Ahsan, O. Fernandez-Delgado, M. Shawky Adly, E.M. Hashem, M. Mahrous Abodouh, M.S. El-Shall, S. T. Sreenivasan, Co–Cu bimetallic metal organic framework catalyst outperforms the Pt/C benchmark for oxygen reduction, J. Am. Chem. Soc. 143 (2021) 4064–4073.
[22] W. Zhou, J. Jia, J. Lu, L. Yang, D. Hou, G. Li, S. Chen, Recent developments of carbon-based electrocatalysts for hydrogen evolution reaction, Nano Energy 28 (2016) 29–43.
[23] Y.-.Y. Ma, C.-.X. Wu, X.-.J. Feng, H.-.Q. Tan, L.-.K. Yan, Y. Liu, Z.-.H. Kang, E.-. B. Wang, Y.-.G. Li, Highly efficient hydrogen evolution from seawater by a low-cost and stable CoMoP@ C electrocatalyst superior to Pt/C, Energy Environ. Sci 10 (2017) 788–798.
[24] M.A. Ahsan, A.R.P. Santiago, A. Rodriguez, V. Maturano-Rojas, B. Alvarado-Tenorio, R. Bernal, J.C. Noveron, Biomass-derived ultrathin carbon-shell coated iron nanoparticles as high-performance tri-functional HER, ORR and Fenton-like catalysts, J. Clean. Prod. 275 (2020), 124141.
[25] M.A. Ahsan, A.R.P. Santiago, M.F. Sanad, J.M. Weller, O. Fernandez-Delgado, L. A. Barrera, V. Maturano-Rojas, B. Alvarado-Tenorio, C.K. Chan, J.C. Noveron, Tissue paper-derived porous carbon encapsulated transition metal nanoparticles as advanced non-precious catalysts: carbon-shell influence on the electrocatalytic behaviour, J. Colloid Interface Sci. 581 (2021) 905–918.
[26] S. Marini, P. Salvi, P. Nelli, R. Pesenti, M. Villa, M. Berrettoni, G. Zangari, Y. Kiros, Advanced alkaline water electrolysis, Electrochim. Acta 82 (2012) 384–391.
[27] M. Zeng, Y. Li, Recent advances in heterogeneous electrocatalysts for the hydrogen evolution reaction, J. Mater. Chem. A 3 (2015) 14942–14962.
[28] I.C. Man, H.Y. Su, F. Calle-Vallejo, H.A. Hansen, J.I. Martínez, N.G. Inoglu, J. Kitchin, T.F. Jaramillo, J.K. Nørskov, J. Rossmeisl, Universality in oxygen evolution electrocatalysis on oxide surfaces, ChemCatChem 3 (2011) 1159–1165.
[29] A.R. Puente Santiago, T. He, O. Eraso, M.A. Ahsan, A.N. Nair, V.S. Chava, T. Zheng, S. Pilla, O. Fernandez-Delgado, A. Du, Tailoring the interfacial interactions of van der Waals 1T-MoS2/C60 heterostructures for high-performance hydrogen evolution reaction electrocatalysis, J. Am. Chem. Soc. 142 (2020) 17923–17927.
[30] A.R. Puente Santiago, M.F. Sanad, A. Moreno-Vicente, M.A. Ahsan, M.R. Cerón, Y.-. R. Yao, S.T. Sreenivasan, A. Rodriguez-Fortea, J.M. Poblet, L. Echegoyen, A New Class of Molecular Electrocatalysts for Hydrogen Evolution: catalytic Activity of M3N@ C2 n (2 n= 68, 78, and 80) Fullerenes, J. Am. Chem. Soc. 143 (2021) 6037–6042.
[31] M. Schalenbach, A.R. Zeradjanin, O. Kasian, S. Cherevko, K.J. Mayrhofer, A perspective on low-temperature water electrolysis-challenges in alkaline and acidic technology, Int. J. Electrochem. Sci 13 (2018) 1173–1226.
[32] H. Dau, C. Limberg, T. Reier, M. Risch, S. Roggan, P. Strasser, The mechanism of water oxidation: from electrolysis via homogeneous to biological catalysis, ChemCatChem 2 (2010) 724–761.
[33] X. Li, X. Hao, A. Abudula, G. Guan, Nanostructured catalysts for electrochemical water splitting: current state and prospects, J. Mater. Chem. A 4 (2016) 11973–12000.
[34] W.T. Hong, M. Risch, K.A. Stoerzinger, A. Grimaud, J. Suntivich, Y. Shao-Horn, Toward the rational design of non-precious transition metal oxides for oxygen electrocatalysis, Energy Environ. Sci. 8 (2015) 1404–1427.
[35] Z. Kato, M. Sato, Y. Sasaki, K. Izumiya, N. Kumagai, K. Hashimoto, Electrochemical characterization of degradation of oxygen evolution anode for seawater electrolysis, Electrochim. Acta 116 (2014) 152–157.
[36] Z. Kato, J. Bhattarai, N. Kumagai, K. Izumiya, K. Hashimoto, Durability enhancement and degradation of oxygen evolution anodes in seawater electrolysis for hydrogen production, App. Surf. Sci. 257 (2011) 8230–8236.
[37] L.Y. Zhang, Z. Liu, B. Xu, H. Liu, Thermal treated 3D graphene as a highly efficient metal-free electrocatalyst toward oxygen reduction reaction, Int. J. Hydrog. Energy 42 (2017) 28278–28286.
[38] N. Komba, Q. Wei, G. Zhang, F. Rosei, S. Sun, Controlled synthesis of graphene via electrochemical route and its use as efficient metal-free catalyst for oxygen reduction, Appl. Catal., B. 243 (2019) 373–380.
[39] C. Fang, J. Zhang, X. Chen, G.J. Weng, Calculating the electrical conductivity of graphene nanoplatelet polymer composites by a Monte Carlo method, Nanomaterials 10 (2020) 1129.
[40] A. Nistal, E. Garcia, D. Pérez-Coll, C. Prieto, M. Belmonte, M. Osendi, P. Miranzo, Low percolation threshold in highly conducting graphene nanoplatelets/glass composite coatings, Carbon N Y 139 (2018) 556–563.

[41] V. Mittal, A.U. Chaudhry, Effect of amphiphilic compatibilizers on the filler dispersion and properties of polyethylene—Thermally reduced graphene nanocomposites, J. Appl. Polym. Sci. 132 (2015).
[42] K. Haubner, J. Murawski, P. Olk, L.M. Eng, C. Ziegler, B. Adolphi, E. Jaehne, The route to functional graphene oxide, ChemPhysChem 11 (2010) 2131–2139.
[43] A.O. Abdelhalim, A. Galal, M.Z. Hussein, I.E.-T. El Sayed, Graphene functionalization by 1, 6-diaminohexane and silver nanoparticles for water disinfection, J. Nanomater. (2016) 2016.
[44] A.B. Bourlinos, D. Gournis, D. Petridis, T. Szabó, A. Szeri, I. Dékány, Graphite oxide: chemical reduction to graphite and surface modification with primary aliphatic amines and amino acids, Langmuir 19 (2003) 6050–6055.
[45] S. Stankovich, R.D. Piner, S.T. Nguyen, R.S. Ruoff, Synthesis and exfoliation of isocyanate-treated graphene oxide nanoplatelets, Carbon N Y 44 (2006) 3342–3347.
[46] P. Wen, Y. Chen, X. Hu, B. Cheng, D. Liu, Y. Zhang, S. Nair, Polyamide thin film composite nanofiltration membrane modified with acyl chlorided graphene oxide, J. Memb. Sci. 535 (2017) 208–220.
[47] V.S. Sapner, B.B. Mulik, R.V. Digraskar, S.S. Narwade, B.R. Sathe, Enhanced oxygen evolution reaction on amine functionalized graphene oxide in alkaline medium, RSC Adv. 9 (2019) 6444–6451.
[48] V.S. Sapner, P.P. Chavan, B.R. Sathe, L-Lysine-Functionalized Reduced Graphene Oxide as a Highly Efficient Electrocatalyst for Enhanced Oxygen Evolution Reaction, ACS Sustain. Chem. Eng. 8 (2020) 5524–5533.
[49] D.C. Marcano, D.V. Kosynkin, J.M. Berlin, A. Sinitskii, Z. Sun, A. Slesarev, L. B. Alemany, W. Lu, J.M. Tour, Improved synthesis of graphene oxide, ACS Nano 4 (2010) 4806–4814.
[50] R. Li, Z. Wei, X. Gou, Nitrogen and phosphorus dual-doped graphene/carbon nanosheets as bifunctional electrocatalysts for oxygen reduction and evolution, ACS Catal. 5 (2015) 4133–4142.
[51] S.Y. Sawant, T.H. Han, M.H. Cho, Metal-free carbon-based materials: promising electrocatalysts for oxygen reduction reaction in microbial fuel cells, Int. J. Mol. Sci. 18 (2017) 25.
[52] F.T. Johra, J.-W. Lee, W.-G. Jung, Facile and safe graphene preparation on solution based platform, J. Indust. Eng. Chem. 20 (2014) 2883–2887.
[53] G. Wang, J. Yang, J. Park, X. Gou, B. Wang, H. Liu, J. Yao, Facile synthesis and characterization of graphene nanosheets, J. Phys. Chem. C 112 (2008) 8192–8195.
[54] S.R.B. Nazri, W.-W. Liu, C.-S. Khe, N. Hidayah, Y.-P. Teoh, C. Voon, H.C. Lee, Adelyn, Synthesis, characterization and study of graphene oxide, in: AIP Conference Proceedings, AIP Publishing LLC, 2018, 020033.
[55] J.-L. Chen, X.-P. Yan, A dehydration and stabilizer-free approach to production of stable water dispersions of graphene nanosheets, J. Mater. Chem. 20 (2010) 4328–4332.
[56] K.M. Aujara, B.W. Chieng, N.A. Ibrahim, N. Zainuddin, C.Thevy Ratnam, Gamma-Irradiation Induced Functionalization of Graphene Oxide with Organosilanes, Int. J. Mol. Sci. 20 (2019) 1910.
[57] K. Zahri, K. Wong, P. Goh, A. Ismail, Graphene oxide/polysulfone hollow fiber mixed matrix membranes for gas separation, RSC Adv. 6 (2016) 89130–89139.
[58] L. Zhang, B. Chen, A. Ghaffar, X. Zhu, Nanocomposite membrane with polyethylenimine-grafted graphene oxide as a novel additive to enhance pollutant filtration performance, Environ. Sci. Technol. 52 (2018) 5920–5930.
[59] J.-l. YAN, G.-j. CHEN, C. Jun, Y. Wei, B.-h. XIE, M.-b. YANG, Functionalized graphene oxide with ethylenediamine and 1, 6-hexanediamine, New Carbon Materials 27 (2012) 370–376.
[60] J.-l. Yan, G.-j. Chen, J. Cao, W. Yang, B.-h. Xie, M.-b. Yang, 1595201. Functionalized graphene oxide with ethylenediamine and 1, 6-hexanediamine, Carbon N Y 52 (2013) 624.
[61] P. Gómez-López, J.Á. Salatti-Dorado, D. Rodríguez-Padrón, M. Cano, C. G. Alvarado-Beltrán, A.R. Puente-Santiago, J.J. Giner-Casares, R. Luque, Mechanochemically Synthetized PAN-Based Co-N-Doped Carbon Materials as Electrocatalyst for Oxygen Evolution Reaction, Nanomaterials 11 (2021) 290.
[62] M. Gong, H. Dai, A mini review of NiFe-based materials as highly active oxygen evolution reaction electrocatalysts, Nano Res. 8 (2015) 23–39.
[63] C. Zhang, B. Wang, X. Shen, J. Liu, X. Kong, S.S. Chuang, D. Yang, A. Dong, Z. Peng, A nitrogen-doped ordered mesoporous carbon/graphene framework as bifunctional electrocatalyst for oxygen reduction and evolution reactions, Nano Energy 30 (2016) 503–510.
[64] T.J. Meyer, The art of splitting water, Nature 451 (2008) 778–779.
[65] Y. Cheng, Advances in electrocatalysts for oxygen evolution reaction of water electrolysis-from metal oxides to carbon nanotubes, Progress Natur. Sci. 25 (2015) 545–553.
[66] M. Busch, N.B. Halck, U.I. Kramm, S. Siahrostami, P. Krtil, J. Rossmeisl, Beyond the top of the volcano?–A unified approach to electrocatalytic oxygen reduction and oxygen evolution, Nano Energy 29 (2016) 126–135.
[67] A. Ambrosi, C.K. Chua, B. Khezri, Z. Sofer, R.D. Webster, M. Pumera, Chemically reduced graphene contains inherent metallic impurities present in parent natural and synthetic graphite, Proc. Natl. Acad. Sci. 109 (2012) 12899.
[68] A. Franco, M. Cano, J.J. Giner-Casares, E. Rodríguez-Castellón, R. Luque, A. R. Puente-Santiago, Boosting the electrochemical oxygen reduction activity of hemoglobin on fructose@ graphene-oxide nanoplatforms, Chem. Commun. 55 (2019) 4671–4674.
[69] Z.K. Ghouri, A. Badreldin, K. Elsaid, D. Kumar, K. Youssef, A. Abdel-Wahab, Theoretical and experimental investigations of Co-Cu bimetallic alloys-incorporated carbon nanowires as an efficient bi-functional electrocatalyst for water splitting, J. Indust. Eng. Chem. 96 (2021) 243–253.
[70] K. Qu, Y. Zheng, Y. Jiao, X. Zhang, S. Dai, S.Z. Qiao, Polydopamine-Inspired, Dual Heteroatom-Doped Carbon Nanotubes for Highly Efficient Overall Water Splitting, Adv. Energy Mater. 7 (2017), 1602068.
[71] J. Lai, S. Li, F. Wu, M. Saqib, R. Luque, G. Xu, Unprecedented metal-free 3D porous carbonaceous electrodes for full water splitting, Energy Environ. Sci. 9 (2016) 1210–1214.
[72] X. Yue, S. Huang, J. Cai, Y. Jin, P.K. Shen, Heteroatoms dual doped porous graphene nanosheets as efficient bifunctional metal-free electrocatalysts for overall water-splitting, J. Mater. Chem. A 5 (2017) 7784–7790.
[73] J. Zhang, L. Dai, Nitrogen, phosphorus, and fluorine tri-doped graphene as a multifunctional catalyst for self-powered electrochemical water splitting, Angew. Chem. 55 (2016) 13296–13300.
[74] T.Y. Ma, S. Dai, M. Jaroniec, S.Z. Qiao, Metal–organic framework derived hybrid Co3O4-carbon porous nanowire arrays as reversible oxygen evolution electrodes, J. Am. Chem. Soc. 136 (2014) 13925–13931.
[75] Y. Xu, W. Tu, B. Zhang, S. Yin, Y. Huang, M. Kraft, R. Xu, Nickel Nanoparticles Encapsulated in Few-Layer Nitrogen-Doped Graphene Derived from Metal–Organic Frameworks as Efficient Bifunctional Electrocatalysts for Overall Water Splitting, Adv. Mater. 29 (2017), 1605957.
[76] B. Bayatsarmadi, Y. Zheng, Y. Tang, M. Jaroniec, S.Z. Qiao, Significant Enhancement of Water Splitting Activity of N-Carbon Electrocatalyst by Trace Level Co Doping, Small 12 (2016) 3703–3711.
[77] Y. Liu, Y. Zhu, J. Shen, J. Huang, X. Yang, C. Li, CoP nanoparticles anchored on N, P-dual-doped graphene-like carbon as a catalyst for water splitting in non-acidic media, Nanoscale 10 (2018) 2603–2612.
[78] C. Lei, H. Chen, J. Cao, J. Yang, M. Qiu, Y. Xia, C. Yuan, B. Yang, Z. Li, X. Zhang, Fe N4 Sites Embedded into Carbon Nanofiber Integrated with Electrochemically Exfoliated Graphene for Oxygen Evolution in Acidic Medium, Adv. Energy Mater. 8 (2018), 1801912.
[79] S. Anantharaj, S. Ede, K. Karthick, S.S. Sankar, K. Sangeetha, P. Karthik, S. Kundu, Precision and correctness in the evaluation of electrocatalytic water splitting: revisiting activity parameters with a critical assessment, Energy Environ. Sci. 11 (2018) 744–771.
[80] F. Song, X. Hu, Exfoliation of layered double hydroxides for enhanced oxygen evolution catalysis, Nat. Commun. 5 (2014) 1–9.
[81] K. Fan, H. Chen, Y. Ji, H. Huang, P.M. Claesson, Q. Daniel, B. Philippe, H. Rensmo, F. Li, Y. Luo, Nickel–vanadium monolayer double hydroxide for efficient electrochemical water oxidation, Nat. Commun. 7 (2016) 1–9.
[82] J. Ortiz-Medina, Z. Wang, R. Cruz-Silva, A. Morelos-Gomez, F. Wang, X. Yao, M. Terrones, M. Endo, Defect engineering and surface functionalization of nanocarbons for metal-free catalysis, Adv. Mater. 31 (2019), 1805717.
[83] C.H. Lee, B. Jun, S.U. Lee, Metal-Free Oxygen Evolution and Oxygen Reduction Reaction Bifunctional Electrocatalyst in Alkaline Media: from Mechanisms to Structure–Catalytic Activity Relationship, ACS Sustain. Chem. Eng. 6 (2018) 4973–4980.
[84] Z. Xie, Y. Wang, Metal-organic framework-derived CoNi-embedded carbon nanocages as efficient electrocatalysts for oxygen evolution reaction, Ion 24 (2018) 1773–1780.
[85] N.-T. Suen, S.-F. Hung, Q. Quan, N. Zhang, Y.-J. Xu, H.M. Chen, Electrocatalysis for the oxygen evolution reaction: recent development and future perspectives, Chem. Soc. Rev. 46 (2017) 337–365.
[86] D.R. Kauffman, D. Alfonso, D.N. Tafen, J. Lekse, C. Wang, X. Deng, J. Lee, H. Jang, J.-s. Lee, S. Kumar, Electrocatalytic oxygen evolution with an atomically precise nickel catalyst, ACS Catal. 6 (2016) 1225–1234.
[87] F. Song, L. Bai, A. Moysiadou, S. Lee, C. Hu, L. Liardet, X. Hu, Transition metal oxides as electrocatalysts for the oxygen evolution reaction in alkaline solutions: an application-inspired renaissance, J. Am. Chem. Soc. 140 (2018) 7748–7759.
[88] J. Duan, S. Chen, M. Jaroniec, S.Z. Qiao, Heteroatom-doped graphene-based materials for energy-relevant electrocatalytic processes, ACS Catal. 5 (2015) 5207–5234.
[89] R.L. Doyle, M.E. Lyons, An electrochemical impedance study of the oxygen evolution reaction at hydrous iron oxide in base, Phys. Chem. Chem. Phys. 15 (2013) 5224–5237.
[90] H.M. Amin, H. Baltruschat, How many surface atoms in Co 3 O 4 take part in oxygen evolution? Isotope labeling together with differential electrochemical mass spectrometry, Phys. Chem. Chem. Phys. 19 (2017) 25527–25536.
[91] S.N. Faisal, E. Haque, N. Noorbehesht, H. Liu, M.M. Islam, L. Shabnam, A.K. Roy, E. Pourazadi, M.S. Islam, A.T. Harris, A quadrafunctional electrocatalyst of nickel/nickel oxide embedded N-graphene for oxygen reduction, oxygen evolution, hydrogen evolution and hydrogen peroxide oxidation reactions, Sustainable Energy & Fuels 2 (2018) 2081–2089.